DE Approach in Development of a Detailed Reaction Network for Liquid Phase Selective Hydrogenation of Methylacetylene and Propadiene in a Trickle Bed Reactor

ARTICLE *in* INDUSTRIAL & ENGINEERING CHEMISTRY RESEARCH · JANUARY 2015

Impact Factor: 2.59 · DOI: 10.1021/ie503600b

4 AUTHORS, INCLUDING:

Fereshteh Samimi

Shiraz University

11 PUBLICATIONS **88** CITATIONS

SEE PROFILE

M. R. Rahimpour

Shiraz University

331 PUBLICATIONS **3,012** CITATIONS

SEE PROFILE

I&EC research
Industrial & Engineering Chemistry Research

Article

pubs.acs.org/IECR

DE Approach in Development of a Detailed Reaction Network for Liquid Phase Selective Hydrogenation of Methylacetylene and Propadiene in a Trickle Bed Reactor

F. Samimi,[†] A. R. Ahmadi,[†] O. Dehghani,[†] and M. R. Rahimpour*[,†,‡]

[†]Department of Chemical Engineering, School of Chemical and Petroleum Engineering, Shiraz University, Shiraz 71345, Iran

[‡]Department of Chemical Engineering and Materials Science, University of California, 1 Shields Avenue, Davis, California 95616, United States

ABSTRACT: Methylacetylene (MA) and propadiene (PD) present in the raw C_3 cut, as the major source of propylene production, are poisonous to catalyst for polymerization plants. So a methylacetylene−propadiene (MAPD) converter is usually required to improve the yield as well as purity of the propylene stream by reduction of the amount of MA and PD present in the raw C_3 cut. In this study, a mathematical modeling is developed for an industrial liquid phase selective hydrogenation of MAPD. In the process model, a new reaction network based on 6 reactions considering green oil formation and unsaturated C_4-cut compounds hydrogenation is proposed. To accomplish this purpose, a Langmuir−Hinshelwood−Hougen−Watson (LH-HW) mechanism is used for this process on an industrial scale. To estimate the reaction rate parameters, the absolute deviations between the model results and the plant data are minimized by applying a differential evolution (DE) optimization technique. To prove the accuracy of the proposed model, simulation results are compared with plant data, and an acceptable agreement is achieved. Then molar flow rates of components, reaction rates profiles, thermal behavior, as well as physical and hydrodynamic properties are verified along the reactor.

1. INTRODUCTION

Thermal cracking of hydrocarbon as well as natural gas results in a wide range of hydrocarbons, among which olefins are the most important ones. Olefins (particularly ethylene and propylene) produced by steam cracking inevitably are contaminated with alkynes and diolefins, which are harmful for later applications.[1] Since the process is rather unselective, a variety of more highly unsaturated compounds have to be removed because of their high reactivity.[2] Therefore, it is necessary to purify the olefins from dienes and alkynes and maximize the productivity of the downstream processes.[1] For this purpose, refining by catalytic selective hydrogenation has gradually increased in importance.[2] For most naphtha-processing plants, the propylene (C_3-cut) stream usually contains more than 90% propylene (PP) and up to 6% methylacetylene (MA) and propadiene (PD),[3] which are poisonous to catalyst for propylene polymerization and would severely reduce the quality of polypropylene.[4] The MAPD removal mechanism was initially established in the gas-phase process. To reduce operating cost and increase competitiveness, the liquid-phase operation has been developed recently in the current petrochemical industry.[3]

MAPD selective hydrogenation was usually addressed via the experimental setup, and some of them have been investigated with regard to several kinds of industrial reactors. However, little work has been performed on the kinetic analysis of selective hydrogenation of MAPD. In 1996, Fajardo et al.[2] studied the gas phase kinetics of hydrogenation of MAPD in a plug-flow reactor over a commercial palladium-based (0.05% Pd/γ-Al_2O_3) catalyst. The rate equations were derived at atmospheric pressure without consideration of green oil formation. The kinetics of MA and PD hydrogenation reactions in the liquid phase was searched by Uygur et al.[5] in 1998 considering three main reactions (MA and PD hydrogenation as well as PR conversion to propane (PN)). Rate equations for MA and PD hydrogenation were described by a reaction mechanism derived according to the LH-HW model. Although the LH-HW was also applied for PR conversion, the errors were very large and the calculated reaction rate values could not reflect satisfactorily the experimental data. Wang and Froment[6] in 2005 developed a kinetic model for the gas phase selective hydrogenation of the C_3-cut of a thermal cracking unit at temperatures 60−80 °C and a pressure of 20 bar. In addition to the hydrogenation reactions, the green oil formation and the catalyst deactivation were also considered in the proposed kinetic model, but the reaction constants and the deactivation parameters were not reported in their study. In 2011, the system identification for a liquid phase selective hydrogenation reactor was accomplished by Wu et al.[7] using a nonlinear regression technique based on an LH-HW kinetic model proposed by Wang and Froment[6] for the gas phase selective hydrogenation of the C_3-cut. Recently Samimi et al.[8] have applied a statistical model in the optimization of an industrial MA and PD hydrogenation reactor. They have investigated the effects of MAPD inlet concentration, fresh feed flow rate, the amount of diluent, and hydrogen flow rates on the propylene production yield by Minitab software.

Although there are several studies in the literature on the subject of reaction schemes, less attention has been paid to

Received: September 11, 2014
Revised: November 30, 2014
Accepted: December 5, 2014
Published: December 22, 2014

DOI: 10.1021/ie503600b
Ind. Eng. Chem. Res. 2015, 54, 117−129

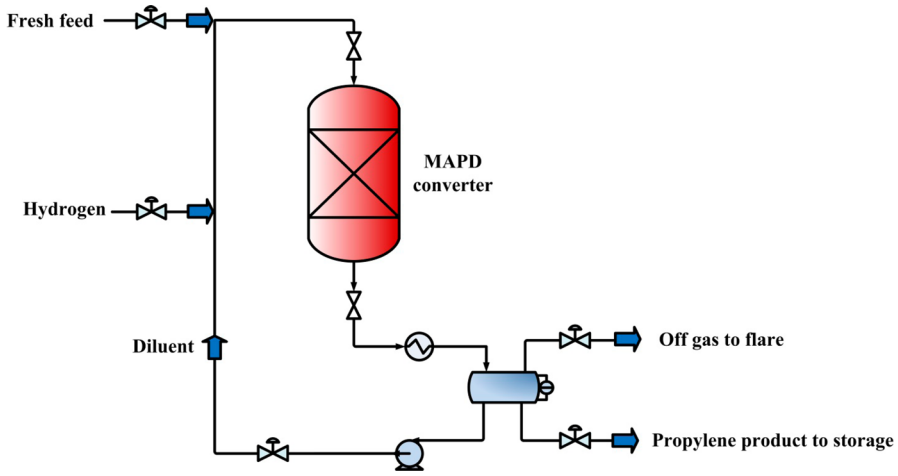

Figure 1. Schematic of an industrial MAPD hydrogenation reactor.

mathematical modeling and simulation of an industrial MAPD hydrogenation reactor. The first step in the modeling of reactors deals with applying an accomplished reaction network which can justify the plant data. As it is clear, there is no suitable reaction network in the literature to determine the kinetics of liquid phase selective hydrogenation of MAPD. So the motivation for this study is to develop a kinetic model to investigate the reactor performance accurately. In this regard, a new reaction network based on 5 components and 1 pseudocomponent as well as 6 reactions, including MA and PD hydrogenation to PR, PR conversion to PN, unsaturated C_4-cut compounds hydrogenation, as well as the green oil formation, is proposed. For this purpose, a LH-HW mechanism was applied for this process on an industrial scale. To estimate the reaction rate constants, the absolute deviations between the model results and the plant data are minimized by applying the differential evolution (DE) optimization method. To prove the accuracy of the proposed model, simulation results are compared with the plant data and an acceptable agreement is achieved.

2. PROCESS DESCRIPTION

Among three-phase gas−liquid−solid reaction systems in the chemical industry, trickle bed reactors (TBRs) are widely used for various hydrogenation reactions because of simple design, reasonable heat transfer efficiency, and low pressure drop. Most commercial TBRs normally operate adiabatically. Operating at elevated temperatures and pressures, they succeed in attaining high conversion per catalyst mass with minimum power consumption that makes them favorable to chemical engineers. In TBRs, gas and liquid phases flow cocurrently or countercurrently through a fixed bed of catalyst particles. However, in most industrial operation downward-flow mode is performed.[9−13]

Figure 1 shows a schematic view of the MAPD hydrogenation unit of a typical olefin plant. The C_3 cut feed is first mixed with the recycle (partially hydrogenated C_3 cut) from the C_3 cut hydrogenation effluent drum in order to decrease the raw C_3 cut reactivity by reducing the concentration of unsaturated components and to increase the space velocity parameter at the reactor inlet. The hydrogen makeup gas is then injected. C_3 cut and H_2 mixture enters the top of the C_3 cut hydrogenation reactor and flows downward through the fixed catalyst bed. The reactor is operated at a pressure of about 24.5 bar and a temperature of 23 °C at the reactor inlet. The reactor effluent is first partially condensed and cooled down in the C_3 cut hydrogenation effluent cooler against cooling water and then goes to the C_3 cut hydrogenation effluent drum. Then a part of the liquid phase is recycled to the reactor by means of the hydrogenated C_3 cut pumps. The operating conditions of the MAPD hydrogenation reactor under the normal conditions are presented in Table 1.

Table 1. Operating Conditions of MAPD Hydrogenation Reactor in the Normal Conditions

Operating conditions	Value
Temperature (K)	296
Pressure (bar)	24.5
Hydrogen flow rate (kg/h)	126
Fresh feed flow rate (kg/h)	46000
Diluent flow rate (kg/h)	45000
Feed Composition (wt %):	
Propylene	88.13
Propane	6.82
MAPD	4.96
1,3-Butadiene	0.01
Butane	0.02
Ethane	0.06
Reactor characteristics:	
Length (m)	3.65
Diameter (m)	1.1
Catalyst properties:	
Particle diameter (mm)	2
Bed void fraction	0.4

3. KINETIC MODELING

3.1. Reaction Network. As mentioned, development of a suitable kinetic model including the main reactions is essential to attain a valid reactor model. Reactor design, process optimization, process control, and cycle length prediction can be performed using a proper kinetic model. So in the present work, by considering all possible reactions, a detailed reaction network is proposed. It should be noted that developing a reaction network including all components with their related reactions is infeasible. So some components are considered as lumped groups. The fresh feed of the reactor is composed of

DOI: 10.1021/ie503600b
Ind. Eng. Chem. Res. 2015, 54, 117−129

MA, PD, PR, PN, and little amounts of unsaturated C4-cut hydrocarbons. Figure 2 shows the proposed reaction scheme,

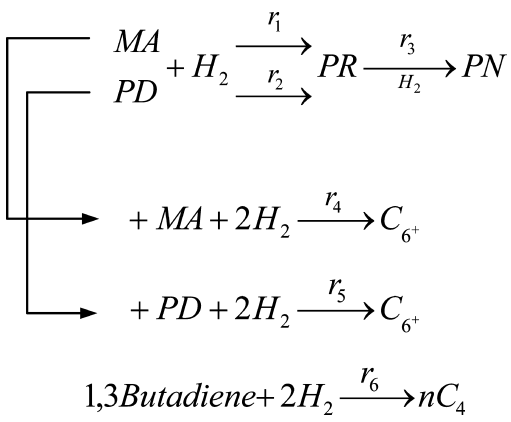

Figure 2. Proposed reaction network for MAPD selective hydrogenation.

including almost all possible reactions with the formation of green oil out of MA and PD as well as hydrogenation of unsaturated C_4-cut compounds. All the reactions are hydrogenation.

3.2. Reaction Criteria. In this research, a Langmuir–Hinshelwood/Hugen–Watson (LH-HW) mechanism is proposed to describe the kinetics of the catalytic reactions. This mechanism is based on the assumption that the adsorption sites are occupied by all reactants (hydrogen and all diolefin or olefin compounds) and that the product molecules are so weakly adsorbed due to the irreversibility of reactions that their surface concentrations are negligible.[14,15]

$$r = k\frac{C_j^a C_{H_2}^b}{\Delta} \tag{1}$$

where

$$\Delta = [1 + K_{H_2}C_{H_2} + K_{MA}C_{MA} + K_{PD}C_{PD} + K_{PR}C_{PR} + K_{1,3\text{-But}}C_{1,3\text{-But}}]^{0.2} \tag{2}$$

C_j and C_{H_2} are the concentrations of diolefin or olefin reactants and hydrogen, respectively. k is the rate constant. K_i represents the adsorption-equilibrium constant of hydrogen and diolefin or olefin reactants at the catalyst surface. a and b are the reaction orders concerning the diolefin or olefin reactants and hydrogen, respectively. The reaction rate constants depend on the temperature, and they are considered to obey the Arrhenius law.

$$k_j = A_j \exp\left(\frac{E_{Aj}}{RT}\right) \tag{3}$$

where A_j represents the frequency factor and E_{Aj} is the activation energy.

The adsorption-equilibrium constants for each reactant are estimated with the Van't Hoff equation. The Van't Hoff equation provides information about the temperature dependence of the adsorption-equilibrium constant.

$$K_j = A_{vj} \exp\left(\frac{-H_j}{RT}\right) \tag{4}$$

A_ν is the adsorption-equilibrium constant at infinite temperature, and H is the adsorption enthalpy.

Generally in fixed-bed reactors with large particle size of catalysts, diffusion within the pores can limit the reaction rate. Also, the superficial fluid velocity may be low enough that the external film resistances become important. In such a situation, the intrinsic kinetics are not applicable. So it is needed to estimate the actual reaction rates. The usual approach is to define the effectiveness factor as below:

$$\eta = (\text{Actual reaction rate})/(\text{Rate predicted from intrinsic kinetic}) \tag{5}$$

The general concept of effectiveness factor is for considering the interaparticle diffusion importance in the porous catalysts.[16] It was observed that a decrease in particle size leads to an increase in the chemical reaction rate.[17] The theoretical calculation of the effectiveness factor was carried out according to a procedure given in the literature.[6]

$$\eta = \frac{1}{\phi}\left[\frac{1}{\tan 3\phi} - \frac{1}{3\phi}\right] \tag{6}$$

Thiele's modulus (ϕ) is used for calculating the effectiveness factor of the catalyst. Smith and Goto[18] represent a generalized Thiele's modulus for an irreversible reaction as follows:

$$\phi = \frac{V_p}{S_p} r(C_s)[2\int_0^{C_s} D_e r dC]^{-1/2} \tag{7}$$

where r is the intrinsic rate of the equation and C is the concentration of limiting component.

3.3. Parameters Estimation. Differential evolution (DE) is an exceptionally simple, a significantly faster, and robust method at numerical optimization and also is more likely to find a function's true global optimum.[19] It can be used for optimizing functions with real variables and many local optimums.[20] Simple structure, ease of use, high speed, and robustness can be counted as DE advantages. It does not require accessory properties such as differentiability and continuity of the objective function.[21] This technique consisted of a main four-step procedure:

- Initialization
- Mutation/perturbation
- Cross over/combination
- Selection

At first (initialization step), an initial population vector, which covers the complete parameters space is selected randomly. Then for each point of the population (named target vector), a mutant vector is produced (mutation/perturbation). In the next step (crossover/combination), mutant vector parameters are combined with one of the target vectors to produce a tail vector, and this vector is substituted as a member, in the next generation, if the function value in the tail vector is less than that in the target vector.

It is obvious that a chosen strategy works differently from one problem to another one. Basically, DE has three key parameters—NP, number of populations; CR, crosses over probability constant; and F, scaling factor—and their choosing depends on the specific problem applied. DE is often difficult, but Price and Storn[19] have given some guiding principles to make it easy. Generally, NP should be about 5–10 times the number of parameters in a vector. F and CR are considered to

DOI: 10.1021/ie503600b
Ind. Eng. Chem. Res. 2015, 54, 117–129

be in the range of 0.4−1 and 0.1−1, respectively. Normally, CR should be as large as possible. The details of the DE algorithm and pseudo-code are available in the literature.[20] The strategy used in this optimization process is "DE/best/1/bin" with the number of population of NP = 240.

In the present work, the reaction rate and adsorption constants, the activation energy, the adsorption enthalpy, as well as the reaction rate powers are considered as the decision variables. Therefore, there are 24 decision variables to be optimized simultaneously. In the present study, 10 data sets of plant (with different operating condition) are used to estimate reaction rate parameters. The ranges of the plant data are presented in Table 2.

Table 2. Ranges of Operating Conditions of Various Days Used for Estimation of Reaction Rate Parameters

Operating condition ranges	Value
Inlet temperature (K)	294.5−296.5
Pressure (bar)	24.5
Hydrogen flow rate (kg/h)	55−140
Fresh feed flow rate (kg/h)	20000−48000
Diluent flow rate (kg/h)	24000−48000
Fresh feed composition range (mol %):	
Propylene	81.00−88.00
Propane	6.00−11.00
MAPD	2.70−6.50
1,3-Butadiene	0.00001−0.0025
Butane	0.001−0.0050
Ethane	0.00053−0.00095
Green oil	0.0000−0.0002
Hydrogen	0.00001−0.0001

The value of NP is set to be 240. Also, the values of the DE step size and CR are chosen to be 0.8. The objective function is considered as

$$OF = \sum_{i=1}^{m} (f_i^{\text{model}} - f_i^{\text{plant}}) + (T^{\text{model}} - T^{\text{plant}}) \quad (8)$$

where f_i represents the outlet molar flow rate. The optimization results are presented in Tables 3−5.

Table 3. Reaction Rate Expressions

	Reaction scheme	Reaction rate criteria (mol/kg cat·s)
1	MA + H_2 → PR	$r_1 = k_1 \frac{C_{MA}^{s\,0.64} C_{H_2}^{s\,0.35}}{\Delta}$
2	PD + H_2 → PR	$r_2 = k_2 \frac{C_{PD}^{s\,0.64} C_{H_2}^{s\,0.35}}{\Delta}$
3	PR + H_2 → PN	$r_3 = k_3 \frac{C_{PR}^{s\,0.64} C_{H_2}^{s\,0.35}}{\Delta}$
4	2MA + 2H_2 → C_{6+}	$r_4 = k_4 \frac{C_{MA}^{s\,0.64} C_{H_2}^{s\,0.35}}{\Delta}$
5	2PD + 2H_2 → C_{6+}	$r_5 = k_5 \frac{C_{PD}^{s\,0.64} C_{H_2}^{s\,0.35}}{\Delta}$
6	1,3-Butadiene + 2H_2 → nC_4	$r_6 = k_6 \frac{C_{1,3\text{-But}}^{s\,0.64} C_{H_2}^{s\,0.35}}{\Delta}$

Table 4. Reactions Rate Constants as Well as Activation Energy

Reaction number	k_i
1	$5.76 \times 10^{-3} \exp\left(\frac{-2286.46}{RT}\right)$
2	$3.60 \times 10^{-3} \exp\left(\frac{-2570.70}{RT}\right)$
3	$8.13 \times 10^{-6} \exp\left(\frac{-3094.48}{RT}\right)$
4	$4.71 \times 10^{-4} \exp\left(\frac{-4510.00}{RT}\right)$
5	$5.99 \times 10^{-4} \exp\left(\frac{-4200.70}{RT}\right)$
6	$6.00 \times 10^{-4} \exp\left(\frac{-4295.67}{RT}\right)$

Table 5. Reaction Rate Adsorption Constants as Well as Adsorption Enthalpy

Component	K_i
H_2	$7.00 \times 10^{-3} \exp\left(\frac{15190.64}{RT}\right)$
MA	$3.50 \times 10^{-3} \exp\left(\frac{25694.14}{RT}\right)$
PD	$2.38 \times 10^{-3} \exp\left(\frac{23700.70}{RT}\right)$
PR	$3.72 \times 10^{-3} \exp\left(\frac{12500.45}{RT}\right)$
1,3-Butadiene	$6.71 \times 10^{-3} \exp\left(\frac{18691.31}{RT}\right)$

4. MATHEMATICAL MODELING

4.1. Assumptions. The following assumptions have been considered in this work:

(1) Reactions occur only at the catalyst surface, and not in the liquid or in the gas phase.
(2) The vaporization of hydrocarbons is not considered due to the operating condition with high pressure and relatively low temperature.
(3) Radial gradients of concentration and temperature are negligible.
(4) Axial dispersion effects are ignored, because of the low gradients of concentration in the commercial units. Therefore, one-dimensional plug flow is considered for both gas and liquid phases.
(5) Catalyst deactivation is ignored.
(6) Intraparticle mass transfer within the pores of the catalyst can be described by the catalyst effectiveness factor.
(7) Nonideal gas phase is considered.
(8) The intraparticle and interphase heat transfer resistances are assumed to be negligible, and liquid and gas are considered as one pseudohomogeneous phase.
(9) The possible temperature gradients inside the catalyst particles and between the catalyst surface and the liquid bulk are not considered.
(10) The reactor operates at steady state under adiabatic conditions, and no heat loss occurs within the reactor.
(11) The trickle flow regime with complete catalyst wetting conditions is considered.

DOI: 10.1021/ie503600b
Ind. Eng. Chem. Res. 2015, 54, 117−129

Figure 3(a) shows the trickle flow regime in which the liquid phase is completely spread over the catalyst surface (catalyst phase is completely wetted), and Figure 3(b) is a computational element with the length of Δz, showing the resistances involved in the liquid phase.

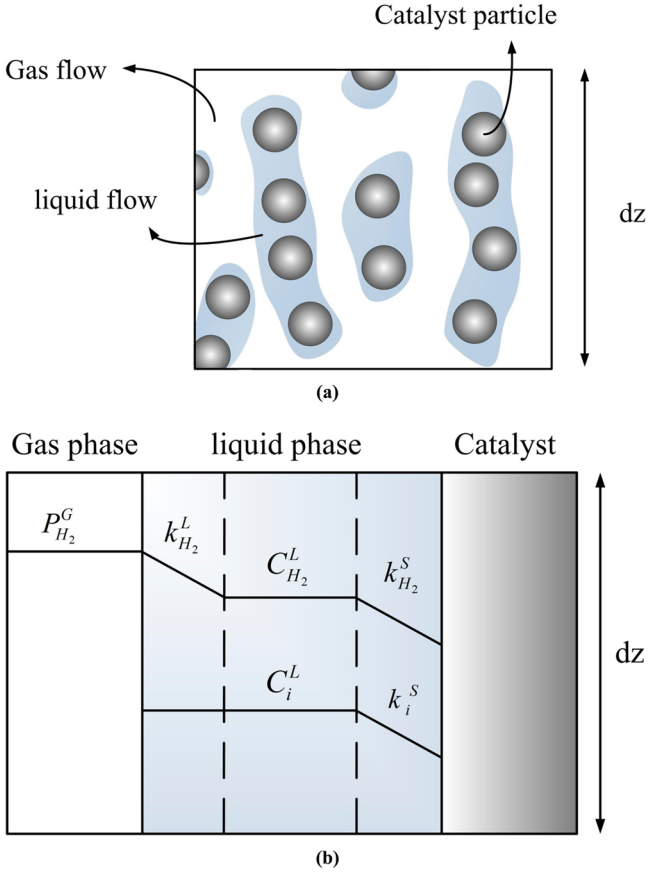

Figure 3. (a) Schematic of a trickle flow regime with completely wetted catalyst in TBR and (b) computational element showing the resistances involved in the liquid phase of TBR.

4.2. Mass and Energy Balance. Using the above-mentioned assumptions, mass balance equations in the trickle bed reactor for diolefin and olefin hydrogenation processes are described with the following set of differential equations:

$$\frac{d\left(u_g \varepsilon_g \frac{P^G_{H_2}}{ZRT}\right)}{dz} = k^L_{H_2} a_l \left(\frac{p^G_{H_2}}{h_{H_2}} - C^L_{H_2}\right) \tag{9}$$

Mass Balance for Hydrogen in the Gas Phase. The initial condition is

$$\text{At } z = 0\text{: } P^G = P^G_0 \tag{10}$$

$$\frac{d(C^L_{H_2} u_l \varepsilon_L)}{dz} = \left[k^L_{H_2} a_L \left(\frac{p^G_{H_2}}{h_{H_2}} - C^L_{H_2}\right) - k^s_{H_2} a_s (C^L_{H_2} - C^s_{H_2})\right] \tag{11}$$

Mass Balance for Hydrogen in the Liquid Phase. The initial condition is

$$\text{At } z = 0\text{: } C^L_{H_2} = C^L_{H_2,0} \tag{12}$$

The above equations represent the mass balance equations for the gaseous component (H_2) while the mass balance equations for the liquid components (MA, PD, PR, 1,3-Butdiene, butane, green oil, and ethane) can be written by equating their liquid-phase concentration gradient to their mass transfer between the liquid and solid phases.

$$\frac{d(C^L_i u_L \varepsilon_L)}{dz} = k^s_i a_s (C^L_i - C^s_i) \tag{13}$$

Mass Balance for Components in the Liquid Phase. The initial condition is

$$\text{At } z = 0\text{: } C^L_i = C^L_{i,0} \tag{14}$$

where i represents MA, PD, PR, 1,3-butadiene, green oil, butane, and ethane.

Mass Balance for Components on the Catalyst Surface. The components transported between the liquid phase and the catalyst surface and within of the catalyst are produced or consumed by the chemical reaction:

$$k^L_i a_s (C^L_i - C^s_i) = \rho_B \sum \eta_j r_j \tag{15}$$

The initial condition is

$$\text{At } z = 0\text{: } C^s_i = C^s_{i,0} \tag{16}$$

where i represents H_2, MA, PD, PR, PN, 1,3-butadiene, butane, green oil, and ethane and j is the number of reactions (1:6).

Energy Balance. Similarly, the energy balance was gotten using the above-mentioned assumptions:

$$\frac{dT}{dz} = [\rho_B \sum \Delta H_j r_j]/[u_G \rho_G Cp_G \varepsilon_G + u_L \rho_L Cp_L \varepsilon_L] \tag{17}$$

The initial condition is

$$\text{At } z = 0\text{: } T = T_0 \tag{18}$$

In order to simulate the reactor, heat and mass transfer between solid and fluid phases have been taken into consideration. Hydrodynamic parameters as well as physical properties of the components are also essential for the calculations. The applied correlations for physical properties are presented in Table 6, and the hydrodynamic parameters are discussed in the following section.

4.3. Hydrodynamic Parameters. Complete understanding of the different hydrodynamic parameters in trickle bed reactors is essential for improvement in design and getting a better performance.

Flow Regime. When gas and liquid flow cocurrently downward through a packed bed of solid particles, different flow regimes were found to occur depending upon the gas and liquid properties, throughputs, operating conditions, and packing characteristics. The four main flow regimes observed are trickle flow, mist flow, bubble flow, and pulsing flow. Knowledge of the flow regime in which the reactor will operate is very important because other hydrodynamic parameters, especially mass transfer rates, are affected by hydrodynamics differently in each regime.[25−27] Most industrial processes operate in trickle flow regime, especially in the processes of hydrogenation, while others operate in pulsing flow regime (e.g., hydrotreating processes) due to the energetic interactions between the phases.[27] Trickle flow is observed at relatively low gas and liquid flow rates and is characterized by liquid phase flowing, driven by gravity, in the form of films or rivulets. The

DOI: 10.1021/ie503600b
Ind. Eng. Chem. Res. 2015, 54, 117−129

Table 6. Auxiliary Correlations

Parameter	Equation
Heat capacities of inorganic and organic liquids for MA, PD, PR, 1,3-Butadiene, and green oil[22] [J/(kmol. K)]	$Cp_L = C_1 + C_2T + C_3T^2 + C_4T^3 + C_5T^4$
Liquid heat capacity for ethane, hydrogen, and propane[22] [J/(kmol. K)]	$Cp_L = \frac{C_1^2}{t} + C_2 - 2C_1C_3t - C_1C_4t^2 - \frac{C_3^2t^3}{3} - \frac{C_3C_4t^4}{2} - \frac{C_4^2t^5}{5}$ $t = 1 - T_r$
Liquid viscosity[22] (Pa·s)	$\mu = \exp\left(C_1 + \frac{C_2}{T} + C_3 \ln T + C_4T^{C_5}\right)$
Gas viscosity[22] (Pa·s)	$\mu = \frac{C_1T^{C_2}}{1 + \frac{C_3}{T} + \frac{C_4}{T^2}}$
Diffusivity of gaseous components[23] (cm^2/s)	$D_{AB}^0 = \frac{117.3 \times 10^{-18}(\varphi M_B)^{0.5}T}{\mu\nu_A^{0.6}}$
Diffusivity of normal paraffin solution[23] (cm^2/s)	$D_{AB}^0 = \frac{113.3 \times 10^{-8}T^{1.47}\eta_B^{\varepsilon}}{\nu_A^{0.71}}$
Diffusion in multicomponent liquid mixtures[23] (cm^2/s)	$D_{Am}^0\eta_m^{0.8} = \sum_{\substack{j=1 \\ j\neq i}}^{n} x_jD_{Aj}^0\eta_j^{0.8}$
Compressibility factor calculation with the Peng–Robinson equation of state[24]	$Z = 1 + \beta - q\beta\frac{(Z - \beta)}{(Z + \varepsilon\beta)(Z + \sigma\beta)}$ $\beta = \Omega\frac{P_r}{T_r}$ $q = \frac{\psi\alpha(T_r)_r}{\Omega T_r}$ $\sigma = 1 + \sqrt{2}$ $\varepsilon = 1 - \sqrt{2}$ $\Omega = 0.07780$ $\psi = 0.45724$ $\alpha(T_r; \omega) = [1 + (037464 + 1.54226\omega - 0.26992\omega^2)(1 - T_r^{1/2})]^2$

continuous gas phase flows through the remaining voids. Pressure drops through the bed remain low, and so the interaction between the gas and liquid phases is referred to as the low interaction regime.[26,28] The flow regime can he divided into two regions. At low gas and liquid flow rates, the liquid flow is laminar and a fraction of the packing remains unwetted. If the liquid rate is raised, the partial wetting regime changes to a complete wetting trickling regime in which the packing is totally covered by a liquid film.[29] There are many flow maps for prediction of flow pattern,[29] but the most important diagram depicting flow regime boundaries has been presented by Charpentier and Favier.[30] Viscosity, surface tension, and density are the important parameters for prediction of flow pattern. The conditions of this work in terms of liquid and gas flow rates, surface tension, density and viscosity of liquid phase, and gas density result in considering the trickle flow regime.

External Wetting Efficiency. The external wetting efficiency (fraction of external area of catalyst effectively wetted by the liquid flowing down the bed) of the catalyst is an important feature in trickle bed operation, as it gives an indication of the extent of catalyst utilization. It is a function of the flow rates of gas and liquid, operating pressure, physical properties of the liquid, and catalyst diameter.[25] Consequently, the external wetting efficiency of a catalyst plays a significant role in the performance of trickle bed reactors.[31] In the trickle flow regime, the catalyst is either completely or partially externally wetted. Many previous studies have been performed to evaluate the wetting efficiency. Mills and Dudukvic[32] presented an equation for wetting efficiency in terms of Weber, Froude, and Reynolds numbers. Generally wetting efficiency depends mainly on the liquid superficial velocity. For liquid superficial velocity lower than 1 (mms^{-1}), the wetting efficiency is smaller than 0.8, and for liquid superficial velocity higher than 4 (mms^{-1}), it is equal to one.[32] Therefore, in a pilot or bench scale reactor, determination of wetting efficiency plays a considerable role while on the industrial scales it is close to unity.

Liquid Hold Up. The liquid holdup is usually defined as the volume of liquid per unit reactor volume. However, for a TBR, liquid holdup is often on the basis of reactor void volume. In a TBR, liquid holdup is divided in two parts, dynamic holdup and static holdup. Dynamic liquid holdup depends mainly on liquid flow rate, liquid properties, and reactor dimensions, while the static holdup depends on the nature of packing, such as porosity and fluid properties. The liquid holdup is considered as one of the main factors oF the reactor performance when the reaction takes place in the liquid phase only. For kinetic analysis, dynamic holdup should be considered.[33]

There are many correlations presented on the evaluation of liquid holdup. Otaka and Okada[33] correlated the dynamic liquid holdup for sphere particles by a relation depending on Reynolds and Galileo numbers as well as particle diameter. Another correlation is presented by Hochman and Effron[34] for

DOI: 10.1021/ie503600b
Ind. Eng. Chem. Res. 2015, 54, 117–129

4.8 mm glass sphere particles and depends only on the Reynolds number. Specchia and Baldi[35] presented two separately correlations. One for poor interaction regime (such as trickle flow regime) and the other for high interaction regime (such as pulse and spray regimes). Since in the present study, the trickle flow regime is considered, the following correlation has been used:

$$h_{dL} = 3.86(\mathrm{Re}_L)^{0.454}(Ga^*)^{-.042}(a_s d_p/\varepsilon)^{0.65} \quad (19)$$

where the liquid-phase Reynolds number, Re_L, is defined in terms of superficial velocity and the modified Galileo number is expressed as below:

$$Ga_L^* = d_p^3 \rho_L(\rho_L g + \delta_{LG})/\mu_L^2 \quad (20)$$

where δ_{LG} is the two phase fractional pressure drops.

Mass Transfer Coefficient. Mass transfer limitations of reactants into the pores of catalyst can be ignored when the catalyst particles are small effectively.[11] In the most cases, the external surface of catalyst is completely wetted, as the total pores are fully filled with the liquid phase due to existence of capillary force.[36] In TBRs (involving liquid and gas flow as well as the solid catalyst particles), interface mass transfer resistances are probably more important than those of simpler fluid−solid catalyst reactors. Therefore, valid information about mass transfer coefficients is often necessary for kinetic modeling or design of TBRs.[37] Goto and Smith,[37] Samb et al.,[38] and Turek and Lang[39] correlated the gas−liquid mass transfer coefficient by physical methods. A correlation was given by Fukushima and Kusaka for estimation of liquid mass transfer coefficient in terms of gas and liquid Reynolds and Schmidt numbers as well as liquid hold up:[40]

$$k_i a_i = \frac{2D_{L,\mathrm{H}_2}(1 - h_{dL})}{d_p^{0.2}} S_p^{.2} \mathrm{Re}_L^{0.73} \mathrm{Re}_G^{0.2} Sc^{0.5} \left(\frac{d_p}{D_i}\right)^{0.2} \quad (21)$$

The liquid−solid mass transfer coefficients in the trickle flow regime can be calculated by the van Krevelen−Krekels equation[41] as follows:

$$\frac{k_i^s}{D_i^L \cdot a_s} = 1.8\left(\frac{G_L}{a_s \mu_L}\right)^{1/2}\left(\frac{\mu_L}{\rho_L D_i^L}\right)^{1/3} \quad (22)$$

where i is H_2, MA, PD, ... and a_s is the specific area of the packing:

$$a_s = \frac{6}{d_p}(1 - \varepsilon) \quad (23)$$

Henry's Constant. The solubility of a gas in a liquid phase depends on temperature, the partial pressure of the gas phase over the liquid phase, the nature of the solvent, and the gas phases. Gas solubility is always limited by the equilibrium between the gas phase and its saturated solution. In this work, mole balance equations based on the gas−liquid equilibrium can be described by Henry's law. Henry's constant (H_{H_2}) can be obtained from the solubility coefficient (λ_{H_2}):[42]

$$H_{\mathrm{H}_2} = \frac{\upsilon_N}{\lambda_{\mathrm{H}_2}\rho_L} \quad (24)$$

Korsten and Hoffmann[43] have presented an equation for the solubility of hydrogen in hydrocarbon mixtures as follows:

$$\lambda_{\mathrm{H}_2} = -0.559729 - 0.42947 \times 10^{-3}T + 3.07539 \times 10^{-3}(T/\rho_L) + 1.94593 \times 10^{-5}T^2 + (0.83578/(\rho_{20})^2) \quad (25)$$

4. NUMERICAL METHOD

The formulated model composed of a set of ordinary differential equations along with associated boundary conditions is considered as an initial value problem. Algebraic equations in the model incorporate initial conditions, reaction rates, as well as aforementioned correlations for the heat and mass transfer coefficients and physical properties of fluids. These equations along with discretized ordinary differential equations using backward finite difference form a set of nonlinear algebraic equations which are solved by the Gauss−Newton method in the MATLAB programming environment.

5. MODEL VALIDATION

The plant data of the adiabatic MAPD hydrogenation reactor for model validation is taken from a domestic petrochemical plant and compared with the modeling result in Table 7. As represented, the modeling results of the reactor are in agreement with the plant data, and the maximum deviation is about 1.49 for outlet temperature, which is an acceptable value.

Table 7. Comparison between the Modeling Results and the Plant Data

Operating condition	Plant data	Model	Error (deviation)
Temperature (K)	329.60	331.09	−1.49
Outlet flow rate (mol/s):			
H_2	1.0727	0.6368	0.4359
MA	0.4525	0.04751	0.40499
PD	0.3014	0.0355	0.2659
PR	549.2416	550.1266	−0.885
PN	41.1085	41.1654	−0.0569
1,3-Butadiene	0.0000	5.4482×10^{-5}	-5.4482×10^{-5}
Butane	0.1304	0.1317	−0.0013
Green oil	1.6565	1.6732	−0.0167
Ethane	0.4965	0.4961	0.0004
Total liquid	594.46049	594.3129	0.14759
Total gas	0.1858	0.18142	0.00438

6. RESULTS AND DISCUSSION

In this section, the predicted molar flow rate of components, reaction rates profiles, thermal behavior, as well as physical and hydrodynamic properties along the TBR are presented. The results are shown in the following sections:

6.1. Molar Behavior. The molar flow rate profile of all components in TBR is depicted in Figures 4 and 5. MA and PD molar flow rates along the reactor are shown in Figure 4(a). As clearly seen, the molar flow rate profile of these compounds is reduced along the reactor bed length. According to Figure 2, MA and PD are consumed to produce PR and green oil. MA and PD molar flow rates decrease severity up to a certain point of the reactor and then will be constant along the TBR configuration. Because at this point the rate of MA and PD hydrogenation reactions will become zero due to the negligible molar flow rate of MA and PD. In fact, the C_3 cut selective hydrogenation system is designed to reduce the amount of MA

DOI: 10.1021/ie503600b
Ind. Eng. Chem. Res. 2015, 54, 117−129

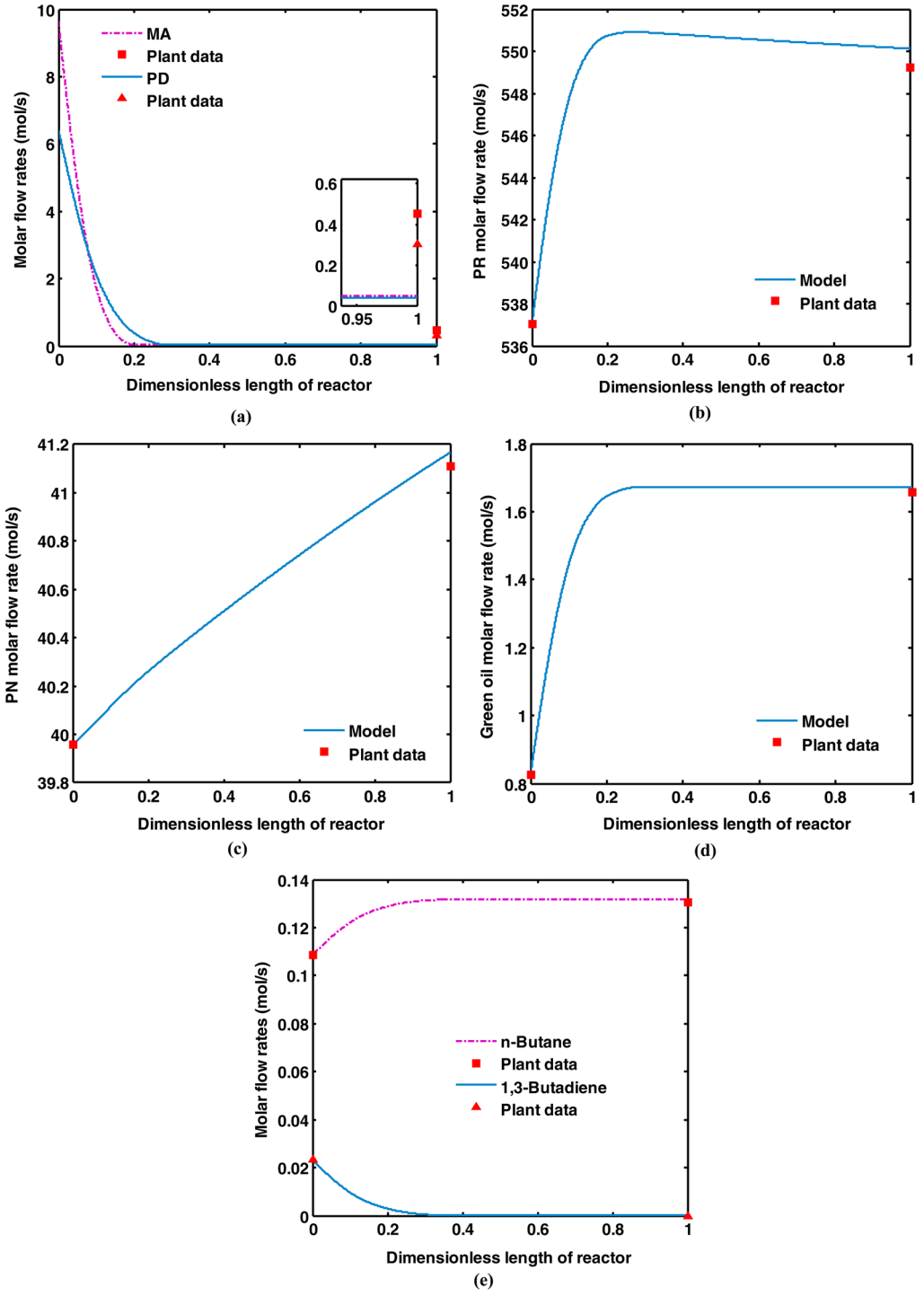

Figure 4. Molar flow rate of (a) MA and PD, (b) PR, (c) PN, (d) green oil, and (e) 1,3-butadiene and *n*-butane along the reactor.

and PD present in the raw C_3 cut from 5 wt % of MAPD to the required product specification of normally less than 2000 ppm wt of MAPD. The modeling results indicate that the outlet MA and PD concentrations are consistent with the required product specification (the plant data for MA and PD are shown with squares and triangles, respectively).

Propylene as the desirable product of the aforementioned reactor is produced from MA and PD hydrogenation reactions according to Figure 2. As depicted in Figure 4(b), PR molar flow rate increases initially due to the hydrogenation of MA and PD in the first part of the reactor and then reaches its maximum value in about 22% of reactor length. At this point, the rate of propylene production becomes zero. After that, the PR molar flow rate follows a decreasing trend along the rest of the reactor length. This behavior is the result of propylene hydrogenation to propane. Despite the selectivity of catalyst, according to Figure 2, some of the propylene in the presence of hydrogen is consumed and converted to propane. Consequently, propane molar flow rate increases up to the end of the reactor (see Figure 4(c)). According to Figure 2, propane is produced in the presence of propylene and hydrogen. If one of these reactants completely is consumed, the rate of propane production will

DOI: 10.1021/ie503600b
Ind. Eng. Chem. Res. 2015, 54, 117−129

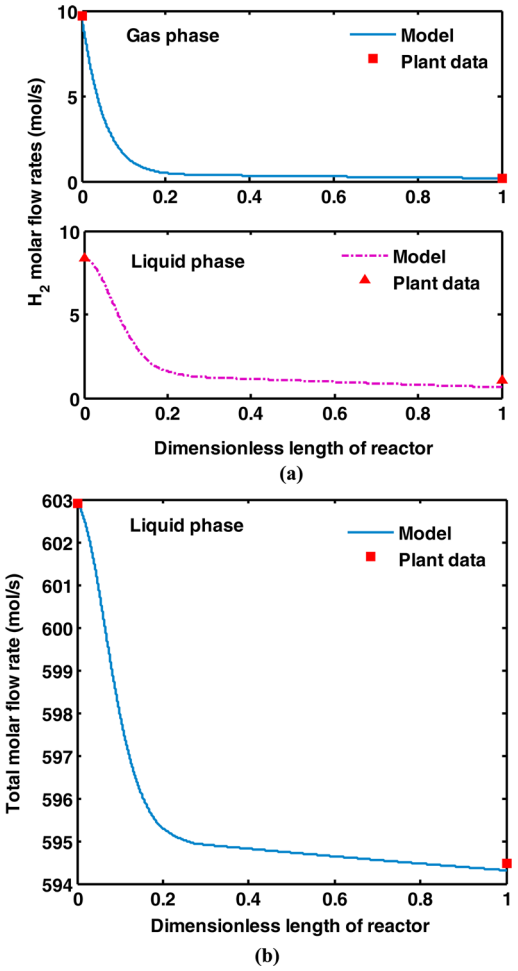

Figure 5. (a) Hydrogen molar flow rate in gas and liquid phases and (b) total molar flow rate of the liquid phase along the reactor.

become zero, and after that propane molar flow rate reaches a constant value up to the end of the reactor. In this reactor, the conversion of PR to PN continues along the reactor bed due to the presence of both propylene and hydrogen up to the end of the reactor.

Green oil (oligomer) as a byproduct of the diolefin hydrogenation process is produced in trace amounts in liquid phase operations owing to removal of produced oligomers from the catalyst surface by the liquid flow. In this industrial reactor, only a small amount of green oil is produced (according to GC analysis, some oligomers were detected). Therefore, they were included in the reaction scheme. In this work, according to the GC analysis, it was found that green oil consists of mainly 6- and 7-carbon compounds (C_6 and C_7). Therefore, for simplicity, a pseudocomponent (C_{6^+}) is defined instead, which includes all these heavy compounds. The molar flow rate profile of green oil is presented in Figure 4(d). In the first part of the reactor, the green oil molar flow rate increases in the presence of a high concentration of MA and PD and then reaches a constant value. It may be a question that green oil increasing in the reactor outlet leads to rapid deactivation of catalysts and reduction of hydrogen injection into the reactor bed. The answer is that the liquid phase operation has superiority to the gas phase process in catalyst life, due to the oligomers washing from the catalyst surface by the liquid flow.

As previously mentioned, the input stream to the reactor contains a small amount of unsaturated C_4 compounds (1,3 butadiene). This component in the presence of hydrogen is consumed and converted to *n*-butane according to Figure 2. As a result, as shown in Figure 4(e), the unsaturated C_4 compounds molar flow rate decreases and the *n*-butane molar flow rate increases.

The molar flow rate profiles of hydrogen in the gas and liquid phases are presented in Figure 5(a), respectively. It is noticed that the hydrogen molar flow rate in the gas phase decreases along the catalyst bed length as a result of hydrogen consumption. Also, the molar flow rate of hydrogen in the liquid phase decreases along the reactor. The significant decrease in the first part of the reactor is because of the high reaction rate of MA, PD, and 1,3-butadien hydrogenations. Since in 30% of the initial length of the reactor, the rate of MA, PD, and 1,3-butadiene hydrogenation as well as green oil formation reactions becomes zero, the hydrogen consumption rate tends to stabilize, but due to the presence of propylene, according to Figure 2, propylene hydrogenation takes place up to the end of the reactor. So, the molar flow rate of hydrogen decreases slightly along the rest of the reactor bed.

The total liquid molar flow rate versus dimensionless length of reactor is shown in Figure 5(b). As seen from this figure, the molar flow rate of the liquid phase has a decreasing trend along the reactor bed. According to Figure 2 one mole olefin or paraffin is produced per two mole of reactants and one mole of green oil is produced per four mole of reactants. So the produced moles are less than the consumed moles. The decreasing trend of total molar flow alters along the reactor bed. This behavior can be described by the difference in reaction kinetics and gas−liquid mass transfer of hydrogen along the reactor. The considerabe decrease in the first part of the reactor is due to the high reactions rate and low mass transfer coefficient in this part. Owing to reducing all the reactions rate (except the rate of propylene hydrogenation to propane) and also because of the high gas−liquid mass transfer coefficient of hydrogen in the rest of the reactor bed, the liquid phase molar flow rate decreases but with a much slower trend.

6.2. Conversion Changes. MAPD conversion to PR and green oil along the reactor is presented in Figure 6. As shown, MAPD total conversion reaches to near 100% in the outlet of the reactor that almost 88% of them is converted to PR and about 12% is converted to green oil.

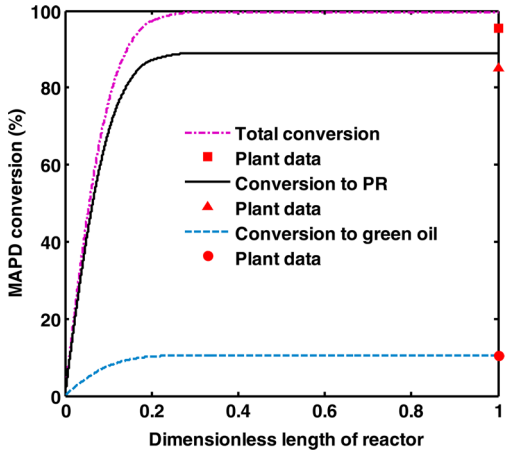

Figure 6. MAPD conversion along the reactor.

DOI: 10.1021/ie503600b
Ind. Eng. Chem. Res. 2015, 54, 117−129

6.3. Reaction Rates. Figure 7 shows the variation of reaction rates. As seen in Figure 7(a), the reaction rates of

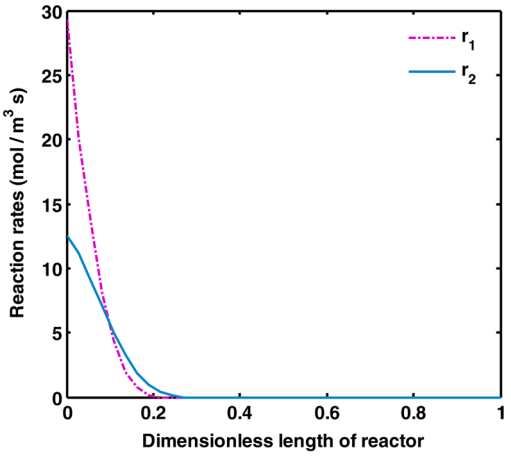

(a)

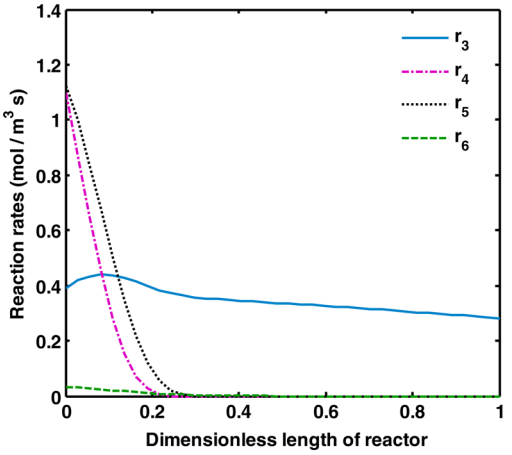

(b)

Figure 7. Reaction rate profiles versus the dimensionless length of the reactor: (a) reactions 1 and 2; (b) reactions 3, 4, 5, and 6.

hydrogenation of MA and PD to PR are reduced rapidly in the first part of the reactor. But after that, the rate of MA and PD hydrogenation decreases slightly to reach zero. The reaction rate criteria (see Table 3) are a function of temperature and reactants concentration. This figure shows that decreasing reactants concentration is dominated over augmentation of temperature.

Figure 7(b) shows the variation of reaction rate of PR and 1,3-butadiene hydrogenation and green oil formation. 1,3-Butadiene hydrogenation and green oil formation reaction rates behave similarly to Figure 7(a). But PR hydrogenation reaction rate behavior is different from other reaction rates in this configuration. It initially increases to reach to its maximum value and then is reduced to the end of the reactor length. This is due to the fact that MA and PD hydrogenation to PR is performed rapidly in the first part of the reactor and the PR molar flow rate reaches its maximum value, but because of the presence of hydrogen in the reactor bed, despite the catalyst selectivity, PR hydrogenation occurs, and with the consumption of PR and hydrogen, the reaction rate decreases up to the end of the reactor.

6.4. Thermal Behavior. Temperature versus dimensionless length of reactor is illustrated in Figure 8. Since the

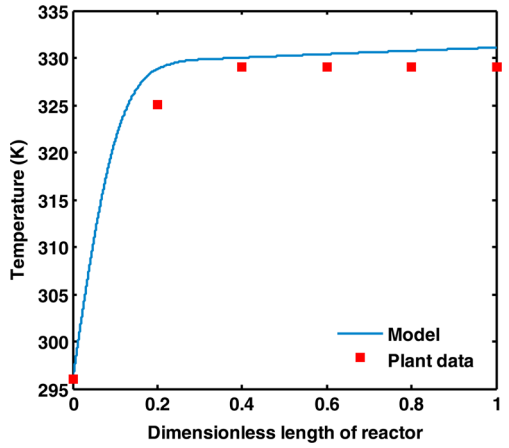

Figure 8. Temperature profiles versus the dimensionless length of the reactor.

hydrogenation reaction is an exothermic irreversible reaction and all the reactions in this configuration are hydrogenation, the reactor temperature will increase along the catalyst bed with different slopes. At the first part of the reactor, temperature increases considerably, owing to MA, PD, and 1,3-butadiene hydrogenation as well as green oil formation. Then, after the completion of these reactions, it tends to be constant, but due to propylene hydrogenation to propane, the temperature increases very slightly in the rest of the reactor. A comparison is also made between the plant data and the model result in this figure. The industrial TBR consists of five different segments to measure the reactor temperature. As seen, the simulation results are in a good agreement with the plant data.

6.5. Hydrodynamic and Physical Parameters. The hydrodynamic and physical properties, including Henry's constant, gas–liquid mass transfer coefficient, liquid and gas hold ups, liquid and gas phase Reynolds numbers, viscosity, and specific heat of the liquid phase profiles in the TBR, are depicted in Figure 9.

Liquid and gas phase hold ups are illustrated in Figure 9(a). As seen, the liquid hold up decreases rapidly initially and then decreases very slightly to the end of the reactor. The liquid hold up in the trickle bed reactor is assumed to depend only on the liquid rate and fluid properties. Since the liquid flow rate and liquid viscosity decrease along the reactor, the liquid to solid ratio is reduced and the liquid hold up decreases. Gas phase hold up has a reverse trend to liquid hold up because the bed void fraction is constant. Thus, by reduction of liquid hold up, gas hold up increases.

Henry's constant and gas–liquid mass transfer coefficient are shown in Figure 9(b). As seen, gas–liquid mass transfer increases along the reactor length, owing to reduction of liquid hold up along the reactor. Because low liquid hold up will offer less liquid phase resistance to the mass transfer of gaseous reactant to the catalyst surface, as a result, the gas–liquid mass transfer coefficient increases. Henry's constant is an inverse function of temperature. In fact, the solubility of gases is reduced as the temperature increases.

Figure 9(c) shows gas and liquid Reynolds numbers variation along the reactor bed. As seen clearly, at the first, the Reynolds number of the liquid phase increases rapidly and then increases slightly. The Reynolds number is a strong function of viscosity (Reynolds number is a reverse function of viscosity), and the liquid phase viscosity is under the influence of temperature. For

DOI: 10.1021/ie503600b
Ind. Eng. Chem. Res. 2015, 54, 117–129

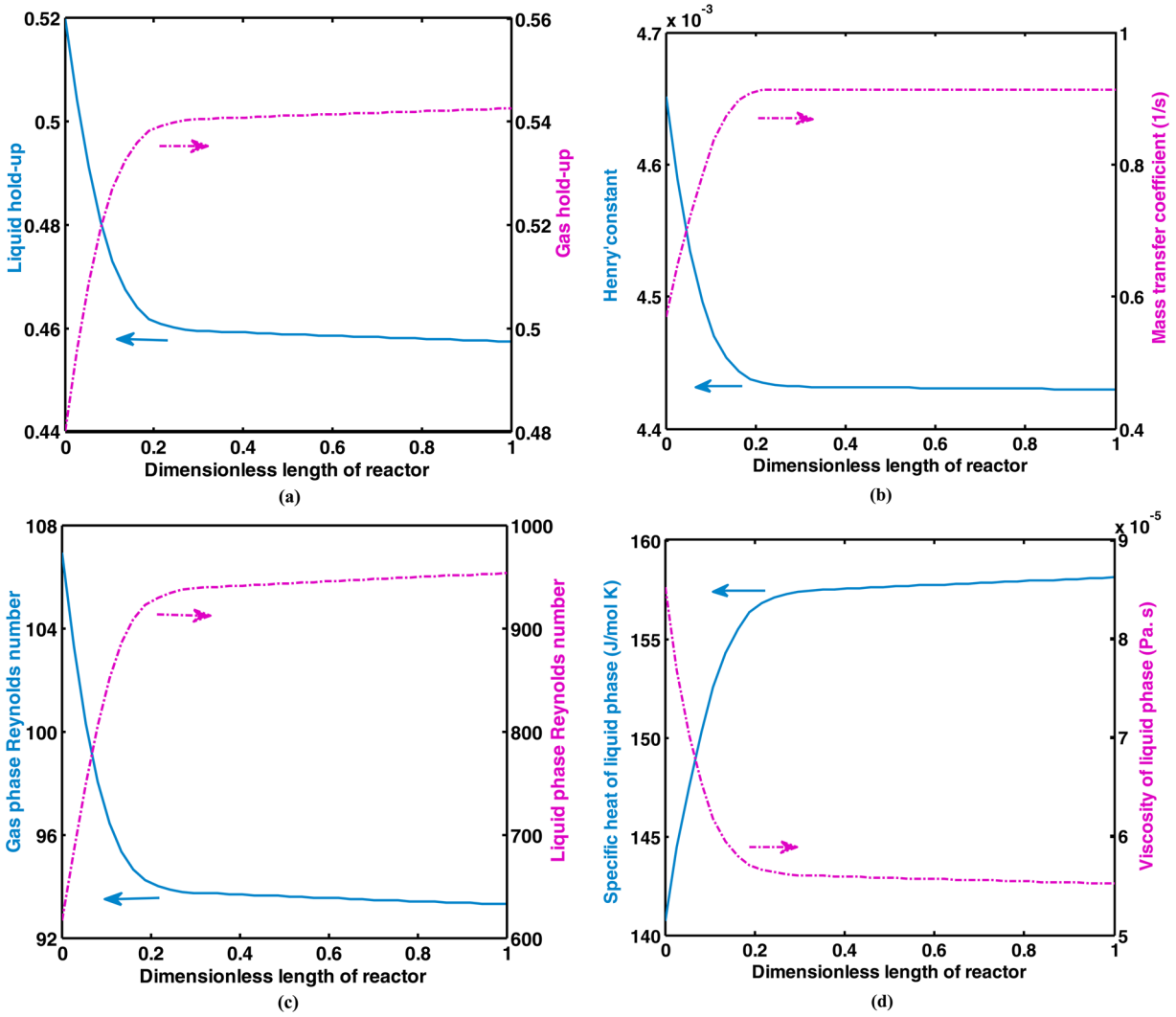

Figure 9. Hydrodynamic parameters: (a) Henry's constant and mass transfer coefficient) and (b) liquid and gas phase hold ups; (c) gas phase and liquid phase Reynolds number; (d) physical parameters along the reactor (specific heat and viscosity of liquid phase).

the liquid phase, by increasing temperature, viscosity is reduced. As a result, the liquid phase Reynolds number increases along the reactor. The gas phase Reynolds number is reduced rapidly and then decreases slightly. The Reynolds number depends on fluid viscosity and velocity. Since the gas phase viscosity increases with the augmentation of temperature (because the molecular momentum exchange force increases with temperature) and also since the gas velocity is reduced as hydrogen is transferred to the liquid phase, consequently, the gas Reynolds number decreases along the reactor bed.

Liquid phase viscosity and specific heat profiles are shown in Figure 9(d). Liquid viscosity and specific heat capacity (see Table 6) are a strong function of temperature and a weak function of composition (since the viscosities of the reactants and products are close to each other and the composition changes are not significant). The liquid phase viscosity is reduced as temperature increases while specific heat increases.

7. CONCLUSION

The aim of this study is mathematical modeling and simulation of an industrial MAPD hydrogenation reactor. To reach this goal, a reaction network was created based on 6 reactions, including MA, PD, PR, and 1,3-butadiene hydrogenation reactions. So, a LH-HW kinetic model was applied and the reaction parameters were estimated using the DE optimization approach. To verify the accuracy of the proposed model, the simulation results were compared with the plant data, and a reasonable agreement was attained. The molar flow rate profile of all components as well as the thermal behavior were investigated, and physical and hydrodynamic parameters were discussed in detail.

AUTHOR INFORMATION

Corresponding Author

*Tel.: +98 713 2303071. Fax: +98 713 6287294. E-mail address: rahimpor@shirazu.ac.ir, mrahimpour@ucdavis.edu.

Notes

The authors declare no competing financial interest.

NOMENCLATURE

a	Order of reaction rate with respect to deolefin or olefin reactants
a_L	Gas−liquid interfacial area, m^{-1}
a_s	Liquid−solid interfacial area, m^{-1}
A_c	Surface area, m^2
A	Pre-exponential factor for reaction j

DOI: 10.1021/ie503600b
Ind. Eng. Chem. Res. 2015, 54, 117−129

A_v Adsorption-equilibrium constant at infinite temperature, mol/m^3
b Order of reaction rate with respect to hydrogen
C_i Concentration of component i, mol/m^3
Cp Specific heat capacity of liquid phase, J/mol K
D_{e_i} Effective diffusivity of i component in the pores of catalyst, m^2/s
d_p Diameter of spherical catalyst particle, m
D_{L,H_2} Molecular diffusivity of hydrogen in liquid phase, m^2/s
D_k Knudsen diffusivity, m^2/s
D_i^L Molecular diffusivity of i component in liquid, m^2/s
D_i Reactor diameter, m
EA_j Activation energy for j reaction, J/mol
f_i Outlet molar flow rates, mol/s
G_L Liquid mass velocity, mol/m^2 s
Ga_L^* Modified Galileo number, dimensionless
g Acceleration of gravity, m^2/s
H_{H_2} Henry's coefficient for hydrogen, bar m^3/mol
H Adsorption enthalpy, J/mol
h_{dl} Liquid holdup, dimensionless
k Rate constants, 1/(mol$^{(a+b-1)}$ kg·cat s)
K Adsorption-equilibrium constant, m^3/mol
$k_{H_2}^L$ Gas−liquid mass transfer coefficient for hydrogen, m/s
$k_{H_2}^s$ Liquid−solid mass transfer coefficient for hydrogen, m/s
k_i^s Liquid−solid mass transfer coefficient for i compound, m/s
L Length of reactor, m
MW Molecular weight, g/g mol
p Reactor total pressure, bar
$P_{H_2}^G$ Partial pressure of hydrogen, bar
R Universal gas constant, J/mol K
Re_L Reynolds number in terms of superficial liquid velocity, dimensionless
Re_G Reynolds number in terms of superficial gas velocity, dimensionless
Sc Schmidt number, dimensionless
s_p Shape factor, dimensionless
S_P Surface area of catalyst, m^2
V_p Volume of catalyst, m^3
T Temperature, K
u_g Superficial velocity of the gas, m/s
u_L Superficial velocity of the liquid, m/s
z Reactor bed length, m
Z Compressibility factor of gas phase, dimensionless

Greek letters

η_j Catalyst effectiveness factor for j reaction, dimensionless
ρ_s Bed density of the catalyst particle, kg/m^3
ρ_L Liquid density at process condition, kg/m^3
ρ_{20} Density of liquid at 20 °C, g/cm^3
ε Void fraction of the catalyst bed, dimensionless
μ_L Liquid viscosity, Pa·s
λ_{H_2} Solubility coefficient of H_2
ΔH_j Heat of j reaction, J/mol
ϕ_i Thiele Modulus of i compound
τ Tortuosity factor
δ_{LG} two phase fractional pressure drop, Pa/m
σ Surface tension, dyn

Superscripts and Subscripts

0 degree
G Gas phase
L Liquid phase
s Solid phase
i Compound (MA, PD, PR, ...)
j Reaction number
p particle

Abbreviations

1,3-But 1,3-Butadiene
CR Cross over probability constant
DE Differential evolution
F Scaling factor
LH-HW Langmuir−Hinshelwood/Hougen−Watson
MA Methylacetylene
NP Number of population
PD Propadiene
PN Propane
PR Propylene
TBR Trickle bed reactor

REFERENCES

(1) Godinez, C.; Cabanes, A. L.; Villora, G. Experimental study of the front-end selective hydrogenation of steam-cracking C_2-C, mixture. *Chem. Eng. Process.* **1996**, *34*, 459−468.
(2) Fajardo, J. C.; Godinez, C.; Cabanes, A. L.; Villora, G. Kinetic analysis of rate data for propylene and methylacetylene Hydrogenation. *Chem. Eng. Process.* **1996**, *35*, 203−211.
(3) Wu, W.; Li, L. Selective Hydrogenation of Methylacetylene and Propadiene in an Industrial Process: A Multiobjective Optimization Approach. *Ind. Eng. Chem. Res.* **2011**, *50*, 1453−1459.
(4) Teixeira, M.; Madeira, L. M.; Sousa, J. M.; Mendes, A. Improving propyne removal from propylene streams using a catalytic membrane reactor−a theoretical study. *J. Membr. Sci.* **2011**, *375*, 124−133.
(5) Uygur, H.; Atalay, S.; Savasci, T. O. Kinetics of liquid phase selective hydrogenation of methylacetylene and propadiene in C3 cut streams. *J. Chem. Eng. Jpn.* **1998**, *31*, 178−186.
(6) Wang, B.; Froment, G. F. Kinetic Modeling and Simulation of the Selective Hydrogenation of the C_3-Cut of a Thermal Cracking Unit. *Ind. Eng. Chem. Res.* **2005**, *44*, 9860−9867.
(7) Wu, W.; Li, Y. L.; Chen, W. S.; Lai, C. C. Kinetic Studies and Operating Strategies for an Industrial Selective Hydrogenation Process. *Ind. Eng. Chem. Res.* **2011**, *50*, 1264−1271.
(8) Samimi, F.; Khadem Modarresi, Z.; Dehghani, O.; Rahimpour, M. R.; Bolhasani, A. Application of response surface methodology for optimization of an industrial methylacetylene and propadiene hydrogenation reactor. *J. Taiwan Inst. Chem. Eng.* **2014**, DOI: 10.1016/j.jtice.2014.09.003.
(9) Larachi, F.; Cassanello, M.; Laurent, A.; Midoux, N.; Wild, G. Gas−liquid interfacial areas in three-phase fixed bed reactors. *Chem. Eng. Process.* **1997**, *36*, 497−504.
(10) Muthanna, H. A. D.; Larachi, F.; Dudukovic, M. P.; Laurent, A. High-Pressure Trickle-Bed Reactors: A Review. *Ind. Eng. Chem. Res.* **1997**, *36*, 3292−3314.
(11) Kostas, C. M.; Nikos, G. P. Kinetics and Mass Transfer of Benzene Hydrogenation in a Trickle-Bed Reactor. *Ind. Eng. Chem. Res.* **2006**, *45*, 7110−7119.
(12) Jakobsson, K.; Hasanen, A.; Aittamaa, J. Modeling of a countercurrent hydrogenation process. *Chem. Eng. Res. Des.* **2004**, *82*, 203−207.
(13) Attou, A.; Boyer, C.; Ferschneider, G. Modelling of the hydrodynamics of the cocurrent gas-liquid trickle ßow through a trickle-bed reactor. *Chem. Eng. Sci.* **1999**, *54*, 785−802.
(14) Carberry, J. J. *Chemical and catalytic reaction engineering*; Science: New York, 2001.
(15) Ertl, G. *Reactions at Solid Surfaces*; Wiley: Hoboken, 2009.
(16) Bischoff, K. B. Effectiveness Factor for General Reaction Rates. *AIChE J.* **1965**, *11*, 351−355.
(17) Aysar, T.; Jarullah, A.; Iqbal, M.; Mujtaba, A. S. W. Kinetic model development and simulation of simultaneous hydrodenitrogenation and hydrodematallization of crude oil in trickle bed reactor. *Fuel* **2011**, *90*, 2165−2181.

DOI: 10.1021/ie503600b
Ind. Eng. Chem. Res. 2015, 54, 117−129

(18) Goto, S.; Smith, J. M. Trickle-Bed Reactor Performance. Part II. Reaction Studies. *AlChE J.* **1975**, *21*, 714−720.
(19) Price, K.; Storn, R. Differential evolution a simple evolution strategy for fast optimization. *Dr. Dobb's J.* **1997**, *78*, 18−24.
(20) Babu, B. V.; Angira, R. Modified differential evolution (MDE) for optimization of non-linear chemical processes. *Comput. Chem. Eng.* **2006**, *30*, 989−1002.
(21) Brest, J.; Greiner, S.; Boskovic, B.; Mernik, M.; Zumer, V. Self-Adapting Control Parameters in Differential Evolution: A Comparative Study on Numerical Benchmark Problems. *IEEE Trans. Evol. Comput.* **2006**, *10*, 646−657.
(22) Bruce, E. P.; George, H. T. Daniel, G. F.; Richard, L. R.; Wilding, W. V. *Perry's chemical engineering handbook*, 8th ed.; McGraw-Hill: 2007.
(23) Bruce E. P; Prausnitz, J. M.; O'Connell, J. P. *The properties of gases and liquids*, 5th ed.; McGraw-Hill: 2001.
(24) Smith, J. M.; Van Ness, H. C.; Abbott, M. M. *Introduction to chemical engineering thermodynamics*, 7th ed.; 2005; pp 96−98.
(25) Prashant, R.; Gunjal, M.N. K.; Vivek, V.; Ranade, R.V. C. Hydrodynamics of Trickle-Bed Reactors: Experiments and CFD Modeling. *Ind. Eng. Chem. Res.* **2005**, *44*, 6278−6294.
(26) Urseanu, M. I.; Boelhouwer, J. G.; Bosman, H. J. M.; Schroijen, J. C.; Kwant, G. Estimation of trickle-to-pulse flow regime transition and pressure drop in high-pressure trickle bed reactors with organic liquids. *Chem. Eng. J.* **2005**, *111*, 5−11.
(27) Al-Naimi, S. A.; Al-Sudani, F. T. J.; Halabia, E. K. Hydrodynamics and flow regime transition study of trickle bed reactor at elevated temperature and pressure. *Chem. Eng. Res. Des.* **2011**, *89*, 930−939.
(28) Munteanu, M. C.; Larachi, F. Flow regimes in trickle beds using magnetic emulation of micro/macrogravity. *Chem. Eng. Sci.* **2009**, *64*, 391−402.
(29) Metaxas, K. C.; Papayannakos, N. G. Kinetics and Mass Transfer of Benzene Hydrogenation in a Trickle-Bed Reactor. *Ind. Eng. Chem. Res.* **2006**, *45*, 7110−7119.
(30) Charpentier, J. C.; Favier, M. Some Liquid Holdup Experimental Data in Trickle-Bed Reactors for Foaming and Nonfoaming Hydrocarbons. *AlChE J.* **1975**, *21*, 1213−1218.
(31) Iliuta, I.; Larachi, F.; Grandjean, B. P. A. Catalst wetting in trickle-flow reactors: A Phenomenological Model, Part A. *Trans IChemE* **1999**, *77*, 759−763.
(32) Mills, P. L.; Dudukovic, M. P. Evaluation of liquid-solid contacting in trickle-bed reactors by tracer methods. *AIChE J.* **1981**, *27*, 893−904.
(33) Shah, Y. T. *Gas-Liquid-Solid reactor Design*, pp 190−192.
(34) Hochman, J. M.; Effron, E. Two-Phase Cocurrent Downflow in Packed Beds. *l&EC Fundam.* **1969**, *8*, 63−71.
(35) Specchia, V.; Baldi, G. Pressure drop and liquid holdup for two phase concurrent flow in packed beds. *Chem. Eng. Sci.* **1997**, *32*, 515−523.
(36) Biardi, G.; Baldi, G. Three-phase catalytic reactors. *Catal. Today* **1999**, *52*, 223−234.
(37) Goto, S.; Levec, J.; Smith, J. M. Mass Transfer in Packed Beds with Two-Phase Flow. *Ind. Eng. Chem., Pracess Des. Bev.* **1975**, *14*, 473−478.
(38) Samb, F. M.; Deront, M.; Adler, N.; Pringer, P. Dynamic liquid holdup and oxygen mass transfer in a cocurrent upflow bioreactor with small packing at low Reynolds numbers. *Chem. Eng. J.* **1996**, *62*, 237−240.
(39) Turek, F.; Lange, R. Mass ransfer in trickle bed reactors at low Reynolds number. *Chem. Eng. Sci.* **1981**, *36*, 569−579.
(40) Fukushima, S.; Kusaka, K. Liquid-Phase Volumetric Mass Transfer Coefficient and Boundary of Hydrodynamics Flow Region in Packed Column with Cocurrent Downward Flow. *J. Chem. Eng. Jpn.* **1977**, *10*, 468−474.
(41) Gilbert, F. F. *Chemical Reactor Analysis and Design*; Wiley: New York,1979.
(42) Aysar, T.; Jarullah, I.M. M.; Wood, A. S. Kinetic model development and simulation of simultaneous hydrodenitrogenation and hydrodemetallization of crude oil in trickle bed reactor. *Fuel* **2011**, *90*, 2165−2181.
(43) Korsten, H.; Hoffmann, U. Three-Phase Reactor Model Pilot Trickle-Bed for Hydrotreating in Reactors. *AIChE J.* **1996**, *42*, 1350−1360.

DOI: 10.1021/ie503600b
Ind. Eng. Chem. Res. 2015, 54, 117−129